Author Manuscript

Author Manuscript

Author Manuscript

Author Manuscript

HHS Public Access

Author manuscript

Mol Psychiatry. Author manuscript; available in PMC 2017 March 24.

Published in final edited form as:

Mol Psychiatry. 2017 April ; 22(4): 585–594. doi:10.1038/mp.2016.102.

Unexpected global impact of VTA dopamine neuron activation as measured by opto-fMRI

Sweyta Lohani, BA[a,1], **Alexander John Poplawsky, PhD**[b,1], **Seong-Gi Kim, PhD**[b,c,d], and **Bita Moghaddam, PhD**[a]

[a]Department of Neuroscience, University of Pittsburgh, Pittsburgh, Pennsylvania, USA

[b]Department of Radiology, University of Pittsburgh, Pittsburgh, Pennsylvania, USA

[c]Center for Neuroscience Imaging Research, Institute for Basic Science, Suwon, 440-330, Korea

[d]Departments of Biomedical Engineering and Biological Sciences, Sungkyunkwan University, Suwon, 440-330, Korea

Abstract

Dopamine neurons in the ventral tegmental area (VTA) are strongly implicated in cognitive and affective processing as well as in psychiatric disorders including schizophrenia, ADHD and substance abuse disorders. In human studies, dopamine-related functions are routinely assessed using functional magnetic resonance imaging (fMRI) measures of blood oxygenation-level dependent (BOLD) signals during the performance of dopamine-dependent tasks. There is, however, a critical void in our knowledge about if and how activation of VTA dopamine neurons specifically influences regional or global fMRI signals. Here we used optogenetics in *Th::Cre* rats to selectively stimulate VTA dopamine neurons while simultaneously measuring global hemodynamic changes using BOLD and cerebral blood volume-weighted (CBVw) fMRI. Phasic activation of VTA dopamine neurons increased BOLD and CBVw fMRI signals in VTA-innervated limbic regions, including the ventral striatum (nucleus accumbens). Surprisingly, basal ganglia regions that receive sparse or no VTA dopaminergic innervation, including the dorsal striatum and the globus pallidus, were also activated. In fact, the most prominent fMRI signal increase in the forebrain was observed in the dorsal striatum that is not traditionally associated with VTA dopamine neurotransmission. These data establish causation between phasic activation of VTA dopamine neurons and global fMRI signals. They further suggest that mesolimbic and non-limbic basal ganglia dopamine circuits are functionally connected and, thus, provide a

Users may view, print, copy, and download text and data-mine the content in such documents, for the purposes of academic research, subject always to the full Conditions of use: http://www.nature.com/authors/editorial_policies/license.html#terms

Address correspondence to: Bita Moghaddam, University of Pittsburgh, Department of Neuroscience, A210 Langley Hall, Pittsburgh, PA 15260, tel: 412 624-2653, fax: 412 624-9198, bita@pitt.edu.

[1]Co-first authors

Conflict of Interest

Authors declare no conflict of interest.

Author Contributions

S.L and A.J.P. performed the experiments and analyzed data. S.L., A.J.P, S.G.K., and B.M. designed the experiments. S.L., A.J.P, and B.M. wrote the paper.

Supplementary information is available at Molecular Psychiatry's website.

Author Manuscript Author Manuscript Author Manuscript Author Manuscript

potential novel framework for understanding dopamine-dependent functions and interpreting data obtained from human fMRI studies.

Keywords

dorsal striatum; nucleus accumbens; optogenetics; basal ganglia; BOLD; CBV; addiction; schizophrenia

Introduction

The mesolimbic dopamine circuitry figures prominently in many models of psychiatric disorders, such as addictive disorders,[1, 2] schizophrenia,[3] and mood and anxiety disorders.[4, 5] Central to this circuitry and the associated disorder models are dopamine neurons in the ventral tegmental area (VTA) that project to the traditional limbic regions, such as the nucleus accumbens (NAc), amygdala and the prefrontal cortex (PFC).[6] The mesolimbic system is generally thought to be functionally distinct from dopamine-innervated basal ganglia regions, including the dorsal striatum (DS), which are implicated in action selection and movement disorders.[7, 8] Accordingly, with a few exceptions,[9, 10] human investigations of addictive disorders,[11] schizophrenia,[12–14] and mood disorders[15, 16] have primarily focused on functional magnetic resonance imaging (fMRI) activity in VTA innervated limbic regions as a measure of dopamine-related dysfunction. Studies of "normal" VTA dopamine-related functions, such as reward prediction error signaling and encoding of motivational salience, in healthy individuals have also focused on these limbic regions, especially the NAc region of the ventral striatum (VS).[13, 17, 18]

Despite the abundance of fMRI studies characterizing normal and abnormal blood oxygenation-level dependent (BOLD) signals in VS and other mesolimbic areas, whether VTA dopamine neuron activity and subsequent dopamine release directly contribute to these BOLD signals is unclear. Most theories on the origin of BOLD signals are centered on glutamate release,[19, 20] and the evidence for dopamine activity contributing to fMRI responses are from indirect observations. For example, systemic administration of psychostimulants, such as amphetamine and cocaine, and D1/D2 agonists/antagonists modulates fMRI signals.[21–23] These effects, however, could be mediated by peripheral/global vascular changes, activation of other adrenergic or serotonergic systems, or alteration of glutamate signaling by psychostimulants.[24] In addition, systemic drug studies cause artificially prolonged changes in dopamine release or receptor activation. This may not model the physiological mechanism of dopamine neuron signaling during behavior, in which dopamine neurons are transiently activated in response to cues and outcomes.[25]

The current study sought to establish causation between phasic activation of VTA dopamine neurons and global fMRI responses in the forebrain. We combined optogenetics with fMRI (opto-fMRI) in *Th::Cre* rats, which allowed us to selectively and transiently stimulate VTA dopamine neurons while simultaneously measuring fMRI signals. We utilized endogenous BOLD contrast for fMRI because of its relevance to neural measures in human studies. The BOLD response, however, may be influenced by nonspecific contributions of large blood vessels.[26] Thus, we also examined cerebral blood volume-weighted (CBVw) fMRI changes

Author Manuscript Author Manuscript Author Manuscript Author Manuscript

using Feraheme as a contrast agent, which reduces sensitivity to large blood vessels and enhances spatial specificity to neural activity.[27, 28] We predicted that the strongest change in fMRI activity would be observed in regions such as the VS that are densely innervated by VTA dopamine neurons. We found, however, that basal ganglia regions such as the DS and globus pallidus (GP) that receive sparse or no VTA dopaminergic innervation were also activated, with activation being much stronger in DS than VS.

Materials and Methods

Animals

Transgenic *Th::Cre* rats that express Cre recombinase under the control of the tyrosine hydroxylase (TH) promoter[29] (gifted by Dr. Karl Deisseroth, Stanford University) and their wild-type litter mates were bred in house by pairing *Th::Cre* rats with wild-type Long Evans rats (Harlan, Frederick, MD). All rats (*Th::Cre*: n = 9, wild-type: n = 4) were housed in a 12-hour reverse light/dark cycle with lights on at 7 pm. All fMRI scans were performed in male adult rats (4–10 months), maintained at ~400 g. Experiments were conducted according to the ethical guidelines of the Institutional Animal Care and Use Committee at the University of Pittsburgh.

Stereotaxic surgery

Under isoflurane anesthesia, *Th::Cre* and wild-type rats were unilaterally injected in the VTA with recombinant adeno-associated viral (AAV) vector constructs containing the gene encoding channelrhodopsin (ChR2) under the Cre promoter (AAV5-Ef1α-DIO-ChR2-eYFP, University of North Carolina Vector Core, Chapel Hill, NC, USA). Four 1 μL injections were made at four VTA sites (AP = 5.0 and 6.0 mm, ML = 0.7 mm, DV = 7.0 and 8.2 mm) (adapted from Witten et al.[29]) at a rate of 0.1 μL min^{-1} using a microsyringe (Hamilton Co., Reno, NV, USA) and a pump (World Precision Instruments, Sarasota, FL). Plastic (240-μm core diameter, 0.63 NA) or silica (200-μm core diameter, 0.22 NA) optical fibers (Doric Lenses, Quebec, Quebec, Canada) were then implanted dorsal to VTA (AP = 5.5 mm, ML = 0.6 – 0.7 mm, and DV = 7.0 – 7.3 mm). All AP/ML and DV measurements are in reference to Bregma and brain surface respectively.[30] Nylon screws (PlasticsOne, Roanoke, VA, USA) and dental cement were used to secure the implant. Optical fibers were implanted either during the viral infusion surgery or ~6 weeks later. All experiments, behavioral and fMRI, were conducted at least 6 weeks after the viral infusion surgeries.

Characterizing virus integration

Post-imaging histology was used to establish colocalization of TH and ChR2-eYFP in dopamine cell bodies (see histology and immunohistochemistry below). All but two *Th::Cre* rats showed sufficient ChR2-eYFP integration in VTA.

Histology and immunohistochemistry

Immediately after the termination of fMRI experiments, animals were anesthetized with an intraperitoneal injection of pentobarbital (120 mg/kg equivalent, Euthasol, Virbac AH, Fort Worth, TX, USA) and transcardially perfused with 0.9% saline and 4% paraformaldehyde (PFA), diluted from 32% PFA solution (Electron Microscopy Sciences, Hatfield, PA, USA).

Author Manuscript Author Manuscript Author Manuscript Author Manuscript

Brains were fixed in 4% PFA overnight at 4°C and then transferred to a 20% sucrose solution. Frozen brains were sectioned at 35 μm, and optical fiber placements in VTA were verified by staining coronal brain slices with cresyl-violet. To examine the expression of ChR2-eYFP in dopamine neurons of VTA, VTA coronal slices were treated with 1% sodium borohydride in 0.1 M sodium phosphate buffer solution (PBS), rinsed with the buffer, and incubated in primary and secondary antibody solutions. The primary antibody solution contained mouse anti-TH antibody (1:2000; #MAB318, EMD Millipore, Billerica, MA, USA), chicken anti-EGFP antibody (1:1000; # ab13970, Abcam, Cambridge, MA, USA), 10% Triton-X and normal donkey serum dissolved in PBS. The secondary antibody solution consisted of Cy3-tagged donkey anti-mouse antibody (1:500; Jackson ImmunoResearch), Alexa Fluor 488-tagged donkey anti-chicken secondary antibody (1:500, Jackson ImmunoResearch, West Grove, PA, USA), 10% Triton-X and normal donkey serum. After antibody reactions, sections were washed in PBS and mounted onto slides. A confocal laser scanning microscope (Olympus Fluoview FV1000, Olympus, Melville, NY, USA) was used to visualize expression of ChR2-eYFP in VTA dopamine neurons. In order to quantify colocalization of TH and EYFP in dopamine cell bodies, Z-stack (step size: 1 μm) images were acquired at 40 X from random locations in the VTA of all *Th::Cre* rats that showed sufficient ChR2-eYFP integration. To better identify EYFP+ cell bodies in the VTA of these rats and accurately determine the specificity of ChR2 expression, slides from a subset of animals (n = 4 *Th::Cre* rats) were further processed with DAPI nuclear staining. These slides were coverslipped with a DAPI-containing mounting medium (Vectashield, Vector Labs, Burlingame, CA), and Z-stack (step size: 1 μm) confocal images were acquired either at 100 X or 40 X combined with 2.5 X True Zoom (Olympus Fluoview FV1000) from random locations in VTA to quantify triple colocalization of TH, ChR2-eYFP and DAPI. Image locations were randomly sampled within the right VTA by manually moving the microscope XY stage, such that the fields of view were non-overlapping and distributed throughout medial, middle and lateral VTA. Image J was used to count the number of cell bodies.

Self-stimulation behavior

Behavior—A subset of rats were tested in an intra-cranial self-stimulation (ICSS) task 2–20 days before the fMRI experiment. While ICSS behavior is a crude measure of dopamine activation and was not used as an inclusion/exclusion criterion, we reasoned that it may provide a pre-histology assessment of virus integration. Behavioral experiments were conducted in an operant box (Coulbourn Instruments, Whitehall, PA, USA) equipped with a nose poke port. Optical fiber implants were connected to a patch cord (200-μm core diameter and 0.22 NA; Doric Lenses, Quebec, Quebec, Canada), attached to a 473-nm blue laser diode (OEM Laser Systems, Midvale, UT, USA) and controlled by a Master-8 stimulator (A.M.P.I., Jerusalem, Israel). Without prior training, rats were given two behavioral sessions over two consecutive days. Each session started as soon as the rats were placed in the operant box and lasted one hour. In the first session, nose poke ports were baited with sugar pellets to facilitate exploration, and nose pokes resulted in blue laser (~473 nm) VTA stimulation (20 Hz, 20 pulses, 5-ms pulse width, 5 – 8 mW output at the optical fiber tip at steady state). In the second session, nose pokes only resulted in VTA stimulation, and sugar pellets were not available.

Author Manuscript Author Manuscript Author Manuscript Author Manuscript

Behavioral data analysis—The total number of nose pokes per session was quantified for each rat. Rats were categorized as behaviorally responsive to stimulation if they executed a total number of nose pokes greater than the upper 99.9% confidence limit of the total nose-pokes executed by wild-type controls in Session 2. Based on this criterion, two *Th::Cre* rats were categorized as behaviorally non-responsive (NB *Th::Cre*), and these were the same rats with poor ChR-eYFP integration in VTA.

Imaging procedures during VTA stimulation

Animal preparation—Rats were induced with 5% and maintained with 2% isoflurane gas in a mixture of 30% O_2 and 70% N_2 gases during surgery. Rats were intubated and mechanically ventilated (TOPO dual mode ventilator, Kent Scientific, Torrington, CT, USA). The ventilation rate was maintained at 55 – 60 breaths/min, while the ventilation volume and ratio of the humidified medical air + O_2 gas mixture were adjusted to maintain oxygen levels at 27 – 28% and end-tidal CO_2 at 3 – 4% (Capnomac Ultima, Datex-Engstrom, Finland). The right femoral artery and vein were catheterized for physiological monitoring and administration of 5% dextrose and contrast agent, respectively. Pancuronium bromide (1 – 2 mg/kg, i.v.) was administered as a muscle relaxant and paralytic.

For hemodynamic measurements, isoflurane was reduced and maintained at 0.7 – 1.0%. The mean arterial blood pressure (MABP) was monitored through the arterial line and was maintained between 70 – 130 mmHg (MP150, BioPac Systems Inc., Goleta, CA, USA). In addition, the rat rectal temperature was maintained at 37 ± 1°C using a warm water circulator, and a 0.9% saline, 5% dextrose, and 0.33 mg/kg/h atropine supplemental fluid was administered intravenously at 1.0 mL/kg/h.

Optical stimulation of VTA—For VTA stimulation, a plastic patch cord (240-μm core diameter, 0.63 NA, 6-m long; Doric Lenses, Quebec, Quebec, Canada), attached to a 473-nm blue laser diode (CrystaLaser, Reno, NV, USA) and controlled by a Master-8 pulse generator (A.M.P.I., Jerusalem, USA), was connected to the implanted optical fiber with a zirconia sleeve (Doric Lenses, Quebec, Quebec, Canada). The light power output was calibrated at the tip of the optical fiber with a broadband power meter (Melles Griot, Carlsbad, CA). The right VTA was stimulated with a pulsed train of light (20 Hz, 5-ms pulse width, 20 s) at an optimal power level (2.5 – 7.5 mW) that elicited maximal activation in downstream areas but did not evoke a MABP change. The same laser power was used for BOLD and CBVw fMRI within the same rat. The onset and offset times for the pulse paradigms were controlled by the MRI acquisition computer.

MRI Experiments—All MRI experiments were performed on a 9.4-T/31-cm MR system interfaced by a DirectDrive console (Agilent Technologies, Santa Clara, CA) and an actively shielded gradient coil with a 40-G/cm peak gradient strength and 120-μs rise time (Magnex, Oxford, UK). The head of the rat was fixed in a non-magnetic head restraint with a bite bar and ear plugs. A custom-built surface coil was placed on the surface of the head and used for radio-frequency excitation and reception.

Author Manuscript Author Manuscript Author Manuscript Author Manuscript

Anatomical MRI—Anatomical images (128 × 128 matrix size, 16 × 16 mm^2 field-of-view (FOV) (125 × 125 μm^2 in-plane resolution)) were acquired using a fast spin-echo sequence and the following parameters: 5.0-s repetition time (TR), train of 8 echoes per segment, 40.7-ms effective echo time (TE), and 4 averages. Seven or 8 1-mm thick slices were acquired with no gap between slices, and the anterior commissure was always centered in the fourth slice.

fMRI data acquisition—We measured two types of fMRI contrasts: endogenous BOLD, followed by contrast-enhanced CBVw fMRI (single i.v. bolus of Feraheme (ferumoxytol, AMAG Pharmaceuticals, Waltham, MA, USA), 15 mg Fe/kg) using a gradient-echo echo-planar imaging sequence with the same FOV as the anatomical images: 16 × 16 mm^2, 64 × 64 matrix size (250 × 250 μm^2 in-plane resolution), 500-ms TR with 2 segments (1-s effective TR), 7 – 8 slices, and 2 dummy scans. The effective TEs were variable for BOLD (12 – 14 ms) and CBVw fMRI (2.5 – 14 ms). We varied the TE values to reduce susceptibility effects (i.e. to improve our baseline signal-to-noise ratio) while still maintaining a high detection sensitivity (i.e. contrast-to-noise ratio) in each animal. The optimal flip angle was determined by acquiring baseline fMRI images at increasing flip angles and selecting the one that had the maximal signal within the striatum. A single fMRI run consisted of 5 baseline (5 s) images followed by 4 concatenated VTA stimulation periods, each consisting of 20 stimulus-evoked (20 s) followed by 40 recovery images (40 s) for a total of 245 images per run.

fMRI data analysis

Data were pre-processed and individual functional maps were calculated using SPM8 (Wellcome Trust Centre for Neuroimaging, London, UK). In addition, a quantitative region-of-interest (ROI) analysis on selected brain regions and a group analysis between rats were performed. Group comparisons were made between wild-type rats and those *Th::Cre* rats with sufficient ChR2 integration in VTA. Data from the *Th::Cre* rats (n = 2) which showed poor ChR2 integration (which were the same rats that were behaviorally non-responsive) were analyzed as a separate group designated as NB *Th::Cre*.

Single animal functional maps—Reconstructed images were spatially realigned, linearly detrended and the normalized difference of the fMRI series (% signal change) was calculated ($[S_t - S_0] / S_0$, where S_0 is the mean of the baseline images and the second half of each of the four recovery periods) using home-written Matlab code (MathWorks, Natick, MA). Motion realignment was performed on a run-by-run basis by co-registering the average S_0 baseline fMRI image of each run to that of the first run using a rigid-body, three degree-of-freedom transformation (3-DOF: translations in x and y-axes, and rotation about the z-axis). Stimulus-evoked increases in CBV cause the raw CBVw fMRI signal to decrease. Therefore, the signs of the CBVw signal changes were reversed so that increased changes represent CBV increases. Repeated fMRI time series of the same stimulation type and parameters were concatenated for subsequent analysis in SPM8.

T-value maps were calculated using a general linear model in SPM8. The fMRI time series × 2 column design matrix consisted of a constant, baseline variable and a predicted

Author Manuscript Author Manuscript Author Manuscript Author Manuscript

hemodynamic response function (HRF) that was calculated by convolving the concatenated block-stimulation paradigm with the default SPM8 BOLD HRF and a previously reported CBVw impulse response function.[31] The effect estimates for each respective variable (β-maps) were then calculated from the pre-processed and concatenated fMRI time series. The resulting β-maps were then used to calculate the t-value functional maps. These functional maps were co-registered to the anatomical images and linearly interpolated to a 128 × 128 matrix size (voxel size: 125 μm × 125 μm × 1 mm) to match the anatomical space.

Baseline signal-to-noise ratio (SNR) and baseline blood volume (BV) index maps were also calculated to examine the influence of these factors on the fMRI activation maps. BOLD and CBVw SNR maps were calculated from the mean of the respective fMRI baseline images (S_0) divided by their standard deviation. BV index maps were calculated from the baseline pre- (pre-S_0) and post- (post-S_0) Feraheme injection images that were acquired with the same TE: ln (pre-S_0 / post-S_0) / TE.[32]

Group analysis—To perform voxel-wise statistical testing across rats, individual functional maps were normalized to a similar anatomical space using SPM8. These transformations were estimated using the anatomical image volumes from each rat, with one representative rat serving as the template. The resulting co-registered anatomical volumes were then averaged and, subsequently, used as the mean anatomical underlay for the group functional maps. Next, the estimated transformations were applied to the corresponding functional maps (previously registered to the anatomical images). The functional maps were then analyzed in SPM8 using one sample t-tests for each group (*Th::Cre* and wild-type) in the 2nd-level analysis to generate group t-maps. A single covariate column for TEs was added in the analysis to exclude the effects of the variable TEs in the group functional maps, although we observed no significant effects of the varied TE for BOLD and only small effects caused by the varied TE for CBVw maps (data not shown). Voxel-wise and family-wise error correction thresholds for *Th::Cre* group maps were set to $p < 0.025$. We chose a moderately conservative voxel-wise threshold of $p < 0.025$ to confidently display meaningful fMRI activations in the *Th::Cre* group maps. We also applied a family-wise correction threshold of $p < 0.025$ (cluster size = 28 voxels) to correct for type-1 errors due to multiple comparisons after voxel-wise statistical tests. To verify that the selected thresholds were appropriate, group maps for *Th::Cre* rats were also generated at other thresholds (voxel-wise = $p < 0.025$, family-wise = none (cluster size = 0 voxels); voxel-wise and family-wise = $p < 0.05$, cluster size = 42 voxels; voxel-wise and family-wise = $p < 0.01$, cluster size = 19 voxels). The appropriate cluster sizes (19, 28 and 48 voxels for family-wise thresholds of $p < 0.01$, $p < 0.025$, and $p < 0.05$, respectively) were determined by the 3dClustSim function in AFNI (Analysis of Functional Neuroimages) software[33] using information about the image sample size and voxel-wise threshold. Group maps for wild-type rats were shown at a low threshold without family-wise error correction (voxel-level $p < 0.025$ and cluster size > 0 voxels) to demonstrate no activation.

ROI analysis—ROIs (ipsilateral and contralateral to the stimulated side) were manually drawn on the high-resolution anatomical images of individual rats and corresponded to the brain regions defined by the Paxinos and Watson[30] brain atlas. Even though group functional

Author Manuscript Author Manuscript Author Manuscript Author Manuscript

maps influenced our choice of ROIs, these ROIs included whole anatomical structures and were drawn blind to the spatial pattern of functional activation within those anatomical regions. DS was also blindly sub-divided into four ROIs (dorsomedial, dorsolateral, ventromedial and ventrolateral). No voxel in the ROI mask was assigned to more than one ROI and some remaining partial volume effects are expected at the ROI boundaries due to the limited spatial resolution of fMRI.

For the ROI analyses, activation t-values (from single animal functional maps), time courses (% signal change across time), SNR, and BV of all voxels (un-thresholded) within each ROI were averaged for each rat. To compare activation t-values between groups (*Th::Cre*, NB *Th::Cre* and wild-type) within each ROI, Brown-Forsythe ANOVAs that do not assume homogeneity of variances were performed. Post-hoc planned comparisons were conducted using two sample t-tests for unequal variances for significant ROIs between a) *Th::Cre* rats and wild-type rats and b) wild-type rats and NB *Th::Cre* rats.

To directly compare the relative t-value, BV, and SNR data across ROIs in the striatum only of *Th::Cre* rats, ROI values were normalized by the sum of the values across the five ROIs for each animal. One-way repeated measures ANOVAs with ROI as the within-subjects factor were then utilized to compare these relative ROI measures across sub-divisions of the striatum, and Greenhouse-Geisser correction was applied whenever necessary. All statistical analyses for ROIs were conducted in SPSS (IBM, Armonk, NY, USA).

fMRI data exclusion criteria—To strictly eliminate controllable sources of hemodynamic contamination in our fMRI data, we removed fMRI runs with stimulation-evoked MABP fluctuations. For this, we correlated the measured MABP time course with the stimulation time course. If the Pearson's correlation was significant at $p < 0.01$ and a MABP change during stimulation was greater than 1 SD from the baseline, then the corresponding fMRI run was removed. A run was excluded if a MABP change was observed during any of the four stimulations or if MABP data were not acquired. This resulted in the exclusion of all BOLD fMRI runs for 2 *Th::Cre* rats. For all other rats, a total of 1 – 6 runs was analyzed per animal and fMRI contrast. One rat was also removed from CBVw group functional maps for *Th::Cre* rats because of poor anatomical image normalization. The resulting sample sizes are depicted in Supplementary Table 1.

Forepaw stimulation

Imaging—Following the completion of VTA stimulation and imaging experiments, additional CBVw fMRI images were acquired for wild-type and NB *Th::Cre* rats during forepaw stimulation to verify that their hemodynamic responses were intact. To stimulate the forepaw, non-magnetic needle electrodes were subcutaneously placed in both forepaws below digits two and four. Rats were maintained at 0.9 – 1.4 % isoflurane, and electrical pulses (1.5 – 3.7 mA, 1 ms stimulus duration, 8 Hz)[34] were delivered to the left and/or right forepaws in a block design (10 – 20 s stimulus on, 50 s recovery, 8 – 12 repetitions). CBVw fMRI images were acquired using the same parameters as VTA stimulation experiments within each animal.

Author Manuscript Author Manuscript Author Manuscript Author Manuscript

Forepaw data analysis—Single animal functional activation maps for forepaw stimulation were calculated similar to VTA stimulation activation maps, as explained in the previous section. For the ROI analysis, contralateral and ipsilateral primary somatosensory cortex (S1) ROIs (in reference to the stimulate forepaw side) were drawn blindly based on anatomical boundaries defined by the Paxinos and Watson[30] atlas. fMRI activation t-values of all voxels (un-thresholded) within the S1 ROIs were averaged for each hemisphere and rat. Since both forepaws (left and right) were simultaneously stimulated for one wild-type rat, the average of both hemispheres served as the contralateral data point, with no ipsilateral reference point. For all other rats contralateral and ipsilateral activation t-values were separately calculated. Then, a two-sample t-test was conducted to compare activation in contralateral and ipsilateral S1.

Results

The experimental design and post-imaging histology results are depicted in Figure 1. *Th::Cre* and wild-type rats received infusions of Cre-dependent AAV viral constructs encoding ChR2 in the VTA before optical fibers were implanted for unilateral optogenetic activation of VTA dopamine neurons (Figures 1A, 1B). After allowing > 6 weeks for viral integration, opto-fMRI experiments were conducted in lightly anesthetized rats (maintained at 0.7 –1 % isoflurane) in a 9.4-T MRI scanner (Figure 1C). Functional images were acquired while VTA was optically stimulated transiently for 20 s at 20 Hz, followed by 40 s of recovery (Figure 1C). We utilized unilateral, as opposed to bilateral, optogenetic control of VTA dopamine activity in combination with fMRI in order to separate ipsilateral, contralateral and bilateral neuronal control.

Post-experiment histology confirmed that optical fibers targeted the right VTA (Figure 1D and Supplementary Figure 1). Viral expression of ChR2 (61% of TH+ cell bodies co-expressed ChR2-eYFP) was highly specific to dopamine neurons in VTA (96% of ChR2-eYFP+ cell bodies also expressed TH) (Figures 1E, 1F and 1G). Activation of VTA dopamine neurons is reinforcing;[29] therefore, to gain a sense that we were sufficiently stimulating dopamine neurons in *Th::Cre* animals, some of the *Th::Cre* and wild-type rats were behaviorally characterized in an ICSS operant task before the opto-fMRI experiments. Out of the rats tested, most *Th::Cre* rats expressed robust ICSS behavior, but two *Th::Cre* rats and all wild-type rats executed very few nose-pokes in this task (Figure 1H). Histology confirmed that the two “behaviorally non-responsive” *Th::Cre* (NB *Th::Cre*) rats expressed low levels of ChR2 in VTA compared to the “behaviorally responsive” *Th::Cre* rats (examples shown in Figure 1H). None of the wild-type rats expressed ChR2 in VTA (example in Figure 1H).

Global fMRI responses to optogenetic stimulation of VTA dopamine neurons

Because of the obvious behavioral and histological separation, NB *Th::Cre* rats were excluded from *Th::Cre* group functional maps and analyzed as a separate “inadvertent control” group in the ROI analysis. Their individual functional maps also showed no activation during VTA optical stimulation for BOLD and CBVw fMRI contrasts (data not shown). Since all other *Th::Cre* rats (including those not characterized in ICSS) showed

Author Manuscript Author Manuscript Author Manuscript Author Manuscript

sufficient ChR2 integration in VTA (comparable to the *Th::Cre* example in Figure 1H) and similar activations in individual functional maps during VTA stimulation, they were included in the *Th::Cre* group analysis.

Group-brain maps—The group analysis revealed that optical stimulation of VTA dopamine neurons in *Th::Cre* rats increased BOLD signals in voxels mostly within the dorsal part of the striatum (Figures 2A, 2B, and Supplementary Figure 2). A few significantly activated voxels were also observed in the VS (includes the NAc), GP, and hippocampus. Since BOLD signals are influenced by baseline CBV,[26] we speculated that the observed robust activation in DS and relatively weak activation in the VS might result from a greater baseline CBV in the dorsal compared to the ventral striatal areas. To address this possibility, we examined fMRI signals using a CBV contrast method. CBVw fMRI has been shown to reduce large vessel artifacts and improve sensitivity around microvessels near the activated neurons.[27, 28] CBVw functional maps for *Th::Cre* rats showed significant activation in response to VTA dopamine stimulation in a larger number of voxels compared to BOLD maps, verifying the improved sensitivity of the CBVw method (Figure 2B, and Supplementary Figure 2). Significant voxels were observed in both DS and VS, orbitofrontal cortex (OFC), medial prefrontal cortex (mPFC), ventral pallidum (VP), GP, hippocampus, amygdala complex, and thalamus. However, activation was still concentrated in the dorsal part of the striatum. There was no significant change in BOLD or CBVw activity throughout the brain of wild-type rats upon optical VTA stimulation (Figure 2C). Activation maps in Figure 2C are shown at a low threshold (no family-wise correction) to demonstrate a lack of any activation. As a positive control, fMRI activation was observed in S1 during forepaw stimulation in wild-type and NB *Th::Cre* rats (Supplementary Figure 3), indicating that their hemodynamic response was intact.

ROI analysis—To complement the group activation maps, we performed ROI analyses using un-thresholded data. The ROIs were chosen based on known output regions of VTA dopamine neurons[6, 35–38] and observed signal changes in group activation maps. A control ROI was also drawn in S1 to assess any non-specific changes from VTA stimulation, given that no activation is expected here. ROIs were drawn as depicted in Figure 2A. Note that the boundaries of VS ROIs were drawn around the NAc, and the olfactory tubercle was excluded.

We examined BOLD activation in ipsilateral (right) forebrain areas that receive substantial projections from VTA dopamine neurons and detected a significant difference between *Th::Cre* and wild-type rats in VS only (Figure 3A). In addition, we observed a significant difference in BOLD activation between *Th::Cre* and wild-type rats in basal ganglia regions —DS and GP— that receive sparse or no projections from VTA dopamine neurons.[6] CBVw activation was significantly different between *Th::Cre* and wild-type rats in many ipsilateral limbic forebrain areas that receive substantial VTA dopaminergic innervation, including VS, VP, OFC, and amygdala, and in regions that receive sparse/no VTA dopamine innervation, such as DS, GP, thalamus and hippocampus[6, 35–38] (Figure 3B). In the contralateral (left) hemisphere, only the thalamus CBVw activation was significantly different between *Th::Cre* and wild-type rats (Supplementary Figure 4). Compared to the right DS activation (t-value >

Author Manuscript Author Manuscript Author Manuscript Author Manuscript

1.5 for BOLD and CBVw), fMRI responses in other regions, including right VS, were much weaker (t-value < 1 for all other ROIs). Because activation was mostly specific to the stimulated hemisphere (except thalamus) and was absent in S1 (Figure 3A and 3B), it is unlikely that the observed BOLD and CBVw responses in *Th::Cre* rats were mediated by residual blood pressure changes, global vascular effects or motion. There was no significant difference in BOLD and CBVw activation between wild-type rats and NB *Th::Cre* rats for any ROI, suggesting that the observed activation patterns were related to the levels of ChR2 in VTA and expression of VTA dopamine stimulation-dependent ICSS behavior.

To further examine the spatial pattern of activation in the striatum of *Th::Cre* rats, we subdivided the right DS into four ROIs. Medio-lateral divisions were drawn as described in the literature.[39, 40] Medial and lateral divisions of the DS are thought to be anatomically and functionally distinct because they receive different inputs and are respectively implicated in associative/limbic versus sensorimotor functions.[39] The medial and lateral divisions were further divided in half to get dorsal and ventral sub-divisions (Figure 3C). Relative activation t-values were significantly different among sub-divisions of the striatum, and the strongest BOLD and CBVw activations upon VTA stimulation were observed in the dorsomedial division, followed by the dorsolateral area of the DS (Figure 3C). The weakest activation was observed in the VS. To determine if baseline SNR and BV can explain the greater activation in DS compared to VS, we compared these factors across striatal subdivisions. Relative BV and SNR for BOLD and CBVw contrasts were significantly different among striatal subdivisions, and the smallest BV and SNR were observed in the VS (Figure 3C). However, a 3.33% average difference in BV and 4.57% (CBVw) to 5.43% (BOLD) average SNR difference between VS and the dorsomedial striatum are unlikely to account for the large difference (24.16 % for BOLD and 21.05 % for CBV, on average) in activation t-values between these regions. In general, in spite of statistically significant differences in BV and SNR, these measures were comparable across striatal subdivisions and may not explain the observed spatial distribution of fMRI activation. However, other possibilities cannot be ruled out, such as differences in neural-hemodynamic coupling mechanisms and/or the dynamic range of activating blood vessels between VS and DS subdivisions.

Time courses—The mean time courses across *Th::Cre* rats from significant ROIs are plotted in Supplementary Figure 5 (no threshold applied). In the right DS, fMRI signals increased gradually and peaked at 1.5 ± 0.2% at 16.8 ± 2.6 s for BOLD and 2.0 ± 0.4% at 18.4 ± 1.6 s for CBVw, respectively. Compared to DS, the peak BOLD and CBVw signal changes in the right VS (BOLD: 1.2 ± 0.2% at 21.6 ± 3.3 s, CBVw: 1.7 ± 0.3% at 24.6 ± 2.4 s) were weaker. Percent signal changes in other activated ROIs were much weaker but exhibited similar slow temporal dynamics in which the signal peaked near the end of stimulation.

Specificity of activation of VTA dopamine neurons

Because of the inevitable spread of virus and ChR2 expression to the adjacent structures, it is possible that some of the observed fMRI activations were mediated by stimulation of dopamine neurons in the SN and other midbrain nuclei. We are, however, confident that we primarily stimulated VTA dopamine neurons for several reasons. First, the optical fiber

Author Manuscript Author Manuscript Author Manuscript Author Manuscript

placements were medial in the VTA of most animals (Supplementary Figures 6 and 7) and, thus, optical stimulation was unlikely to have strongly activated SN neurons. Second, regardless of the exact VTA optical fiber placement, we consistently observed a striking DS activation in the individual maps of all *Th::Cre* rats (excluding NB *Th::Cre* rats, example activation maps for two rats shown in Figure 4). This point is further demonstrated by directly comparing striatal activation between two rats with medial and lateral placements of optical fibers in VTA (Figure 4). Because of the very medial location of the fiber tip in rat #3460 and low laser output (power = 2.5 mW at fiber tip, irradiance = 1.83 mW/mm^2 at 500 μm from fiber tip), it is highly unlikely that SN dopamine neurons were activated during optical stimulation of VTA. The predicted blue light irradiance during stimulation even at the medial edge of SN was < 0.47 mW / mm^2, which is not sufficient to elicit action potentials [41]. However, optical stimulation robustly increased CBVw activity in the DS of this rat (Figure 4A). In contrast, because of the lateral location of the fiber tip and higher laser output (power = 5 mW at fiber tip, irradiance = 3.66 mW/mm^2 at 500 μm from fiber tip) in rat #3446 (Figure 5B), there was a greater possibility of activating SN dopamine neurons with stimulation. Activation maps of this rat still revealed strong CBVw activation in the DS. The similarity of the fMRI activation maps between these two rats further indicates that weaker VS versus stronger DS activation is not due to preferential stimulation of SN dopamine neurons.

Discussion

The current study establishes causation between activation of VTA dopamine neurons and fMRI responses in VTA dopamine-innervated limbic regions that include the VS, VP, OFC, and amygdala. fMRI activation was also observed in regions that do not receive substantial VTA dopamine projections, such as thalamus, hippocampus, and basal ganglia regions (DS and GP).[6, 35–38] In particular, DS exhibited the most robust BOLD and CBVw signal increase, compared to other regions, upon activation of VTA dopamine neurons. These results, thus, suggest a potentially novel dynamic VTA–basal ganglia circuit associated with phasic activation of VTA dopamine neurons.

Contribution of dopamine neuron activation to hemodynamic signals

The most straightforward explanation for the observed hemodynamic changes in downstream areas that receive dense dopamine innervation from the VTA, including VS, is enhanced local dopamine release. We, however, also observed significant fMRI activation in regions, such as the DS and GP, that are not traditionally considered part of the VTA dopaminergic system.[8] Although a recent study identified considerable collateral projections from VTA dopamine neurons to medial and lateral DS,[42] decades of tracing studies have indicated that VTA dopamine neurons send sparse projections to DS, most of which terminate in the very medial edge of DS and none in GP.[6] Furthermore, optogenetic stimulation of VTA dopamine neurons elicits phasic dopamine release selectively in VS and not in DS.[43] Hence, given the robust fMRI activation in DS that is two-times larger compared to the response in VS, local dopamine release from direct dopaminergic projections cannot entirely explain the observed fMRI signals in DS.

Author Manuscript Author Manuscript Author Manuscript Author Manuscript

In light of recent studies indicating that selective activation of dopamine fibers elicits net inhibition in striatal projections neurons,[44, 45] it is further unlikely that dopamine projections to the striatum monosynaptically mediate the robust fMRI activation in this region. In fact, fMRI activations are primarily attributed to changes in glutamate neurotransmission; blockade of local glutamate receptors profoundly reduces hemodynamic fMRI signals,[46] and > 80% of glucose metabolism in the rat cortex is estimated to be due to glutamate release and uptake.[47] Given this body of evidence, we propose that the robust fMRI response in DS is mediated, at least in part, by network-level interactions involving long-range basal ganglia-thalamic-cortical loops that may terminate in the striatum via convergent glutamate projections.[48, 49] There are several potential networks that may be involved. For example, VTA dopamine modulation of VS neurons can influence thalamic neurons (directly or indirectly via the pallidum).[48, 50] A change in thalamic activity may then influence DS fMRI signals via direct thalamic glutamate projections or via modulation of cortical efferents to the DS.[49] This proposed divergence of signal from the VS to thalamic and cortical areas and eventual convergence of glutamatergic inputs to the DS may amplify fMRI responses in this region. Consistent with this potential mechanism, we observed significant fMRI responses to VTA dopamine stimulation in the thalamus, pallidum, and cortical areas such as the OFC. Further studies including pharmacology and recording from DS and thalamic/cortical neuronal ensembles are necessary to delineate this proposed mechanism.

Of note, a recent study reported that activation of VTA dopamine neurons did not greatly increase forebrain BOLD fMRI signals,[51] in contrast to our observations in the present study. We speculate that differences in the anesthesia choice and depth, lower BOLD sensitivity at the 4.7-T magnetic field, and length of VTA stimulation (8 s compared to 20 s) may contribute to this discrepancy. The latter possibility may play a significant role because the VTA stimulation-dependent activation time courses that we observed were very slow, and activation tapered off soon after the stimulus offset. In the current experiment, the percent BOLD signal change in DS was only 0.47 ± 0.24% at 8 s, which is expected to be less at 4.7-T and may be below the limits of detection.

Functional relevance of VTA - DS activation

Mesolimbic projections from VTA and nigrostriatal projections from SN are generally thought to be distinct dopaminergic systems that modulate processes mediated by VS and DS, respectively.[6, 8, 52] While the lack of clear separation between VTA and SN and their projection targets has also been recognized,[6] the present finding that activation of VTA dopamine neurons robustly increases DS fMRI activity suggests that there is considerable functional overlap between mesolimbic and nigrostriatal systems. Thus, activation of VTA dopamine neurons may influence classic non-limbic basal ganglia-related motor/cognitive functions. It is interesting that within the DS, stronger activation was observed in dorsal areas, with the medial dorsal half exhibiting slightly greater activation than the lateral dorsal half. The medial (associative striatum) and lateral (sensorimotor striatum) divisions of DS receive different cortical and sub-cortical inputs and are involved in “cognitive control” functions and goal-directed motor-learning versus expression of habitual/skilled behaviors, respectively.[7, 39] Further studies are necessary to determine the relation of the activation

Author Manuscript Author Manuscript Author Manuscript Author Manuscript

pattern within DS to the topography of inputs to DS and the functional consequence of VTA dopamine activation in associative/cognitive versus habitual behaviors.

Relevance to human neuroimaging and psychiatric disorders

The existence of a functional VTA ->DS/GP circuit has implications for disorders that are traditionally associated with either the mesolimbic or non-limbic basal ganglia regions. For example, schizophrenia is considered primarily a disorder of the VTA dopaminergic system, and animal models of schizophrenia heavily focus on VTA innervated regions, in particular the VS/NAc.[3, 53] Human imaging studies, however, have shown abnormal hemodynamic activity in DS as well as VS in schizophrenia.[13, 54–57] Recent studies have further implicated dopamine neurotransmission in the associative regions of the DS, but not VS, in schizophrenia and the vulnerability to develop the disorder.[58, 59] While the human DS findings may have been interpreted as a departure from the involvement of limbic circuits in the pathophysiology of schizophrenia,[58] the present data suggest that the DS dysfunctions are consistent with the “mesolimbic dopamine hypothesis” of schizophrenia.

Similarly, although most animal research on addiction focuses on the VTA to VS/NAc circuit, abnormal fMRI activity is observed in both DS and VS in addictive disorders.[1, 11, 60, 61] Only recently has the crucial role of DS in addiction been recognized, and this has been explained in terms of alterations in mesostriatal projections from SN.[11] Our data, however, suggest that DS abnormalities in addiction could result directly from cellular adaptations in and aberrant activation of VTA dopamine neurons. Evidence of heightened BOLD activity in both DS and VTA but moderate activation in NAc of heavy drinkers compared to social drinkers during exposure to alcohol-related cues[60] supports the idea of an aberrant VTA to DS circuit in addiction.

Methodological considerations

Several potential methodological concerns should be addressed. First, a recent study reported significant ectopic Cre expression in the VTA of *Th::Cre* mice,[62] suggesting that optogenetic stimulation in *Th::Cre* transgenic lines may activate non-dopamine cells. The *Th::Cre* rat strain we used here, however, is a different genetic line, and we and others[29] have observed very little ectopic expression of ChR2 in the VTA of these rats. Thus, it is unlikely that our results are due to significant activation of non-dopamine VTA neurons.

Second, optogenetic stimulation of VTA dopamine neurons is, obviously, an artificial method of activation and may result in synchronous firing of a large group of dopamine neurons. This may not represent the spatial and temporal dynamics of VTA neuron firing that we typically observe during task performance.[63, 64] Regardless, the results of the current study are important because they highlight the existence of VTA dopamine-dependent dynamic circuits that may come online during certain behaviors or pathological conditions.

Finally, the choice and level of anesthesia could have impacted our observed fMRI activation maps. For example, isoflurane anesthesia suppresses BOLD fMRI activation,[65] which could explain the paucity of significant BOLD activations outside the striatum in the present study. We accounted for some of this anesthesia-induced reduction in sensitivity by the use of a CBV contrast that dramatically increased fMRI activations in many areas.

Author Manuscript Author Manuscript Author Manuscript Author Manuscript

Conclusions

Optogenetic stimulation of VTA dopamine neurons increased fMRI signals in regions, such as the VS, that are directly innervated by these neurons. Concomitant activation was observed in the dorsal striatal and pallidal regions of the basal ganglia that do not receive considerable dopamine innervation from the VTA. These results suggest a functional interaction between phasic activation of VTA dopamine neurons and basal ganglia systems, providing a novel circuit-level framework that may be critical for reassessing existing theoretical models about striatal-dependent normal functions and brain disorders such as schizophrenia and substance abuse disorder.

Supplementary Material

Refer to Web version on PubMed Central for supplementary material.

Acknowledgments

This work was supported by the National Institutes of Health grants R01 (MH048404 and EB003324), R21 (EB018903), Multimodal Neuroimaging Training Fellowship (University of Pittsburgh), and the Institute for Basic Science (IBS-R015-D1).

References

1. Koob GF, Volkow ND. Neurocircuitry of addiction. Neuropsychopharmacology. 2010; 35(1):217–238. [PubMed: 19710631]
2. Everitt BJ, Belin D, Economidou D, Pelloux Y, Dalley JW, Robbins TW. Review. Neural mechanisms underlying the vulnerability to develop compulsive drug-seeking habits and addiction. Philosophical transactions of the Royal Society of London Series B, Biological sciences. 2008; 363(1507):3125–3135. [PubMed: 18640910]
3. Grace AA. Gating of information flow within the limbic system and the pathophysiology of schizophrenia. Brain research Brain research reviews. 2000; 31(2–3):330–341. [PubMed: 10719160]
4. Nestler EJ, Carlezon WA Jr. The Mesolimbic Dopamine Reward Circuit in Depression. Biological Psychiatry. 2006; 59(12):1151–1159. [PubMed: 16566899]
5. Polter AM, Kauer JA. Stress and VTA synapses: implications for addiction and depression. Eur J Neurosci. 2014; 39(7):1179–1188. [PubMed: 24712997]
6. Bjorklund A, Dunnett SB. Dopamine neuron systems in the brain: an update. Trends Neurosci. 2007; 30(5):194–202. [PubMed: 17408759]
7. Graybiel AM, Grafton ST. The striatum: where skills and habits meet. Cold Spring Harbor perspectives in biology. 2015; 7(8):a021691. [PubMed: 26238359]
8. Smith Y, Kieval JZ. Anatomy of the dopamine system in the basal ganglia. Trends in Neurosciences. 2000; 23(Supplement 1):S28–S33. [PubMed: 11052217]
9. Howes OD, Williams M, Ibrahim K, Leung G, Egerton A, McGuire PK, et al. Midbrain dopamine function in schizophrenia and depression: a post-mortem and positron emission tomographic imaging study. Brain. 2013; 136(Pt 11):3242–3251. [PubMed: 24097339]
10. Yoon JH, Minzenberg MJ, Raouf S, D'Esposito M, Carter CS. Impaired Prefrontal-Basal Ganglia Functional Connectivity and Substantia Nigra Hyperactivity in Schizophrenia. Biol Psychiatry. 2013
11. Volkow ND, Wang GJ, Fowler JS, Tomasi D. Addiction circuitry in the human brain. Annu Rev Pharmacol Toxicol. 2012; 52:321–336. [PubMed: 21961707]

Author Manuscript Author Manuscript Author Manuscript Author Manuscript

12. Juckel G, Schlagenhauf F, Koslowski M, Wustenberg T, Villringer A, Knutson B, et al. Dysfunction of ventral striatal reward prediction in schizophrenia. Neuroimage. 2006; 29(2):409–416. [PubMed: 16139525]
13. Morris RW, Vercammen A, Lenroot R, Moore L, Langton JM, Short B, et al. Disambiguating ventral striatum fMRI-related bold signal during reward prediction in schizophrenia. Molecular Psychiatry. 2012; 17(3):280–289.
14. Rolland B, Amad A, Poulet E, Bordet R, Vignaud A, Bation R, et al. Resting-state functional connectivity of the nucleus accumbens in auditory and visual hallucinations in schizophrenia. Schizophr Bull. 2015; 41(1):291–299. [PubMed: 25053649]
15. Nauczyciel C, Robic S, Dondaine T, Verin M, Robert G, Drapier D, et al. The nucleus accumbens: a target for deep brain stimulation in resistant major depressive disorder. Journal of Molecular Psychiatry. 2013; 1(1):17. [PubMed: 26019865]
16. Arrondo G, Segarra N, Metastasio A, Ziauddeen H, Spencer J, Reinders NR, et al. Reduction in ventral striatal activity when anticipating a reward in depression and schizophrenia: a replicated cross-diagnostic finding. Front Psychol. 2015; 6:1280. [PubMed: 26379600]
17. O'Doherty JP, Dayan P, Friston K, Critchley H, Dolan RJ. Temporal Difference Models and Reward-Related Learning in the Human Brain. Neuron. 2003; 38(2):329–337. [PubMed: 12718865]
18. Carter RM, Macinnes JJ, Huettel SA, Adcock RA. Activation in the VTA and nucleus accumbens increases in anticipation of both gains and losses. Frontiers in behavioral neuroscience. 2009; 3:21. [PubMed: 19753142]
19. Attwell D, Buchan AM, Charpak S, Lauritzen M, Macvicar BA, Newman EA. Glial and neuronal control of brain blood flow. Nature. 2010; 468(7321):232–243. [PubMed: 21068832]
20. Lauritzen M. Reading vascular changes in brain imaging: is dendritic calcium the key? Nat Rev Neurosci. 2005; 6(1):77–85. [PubMed: 15611729]
21. Knutson B, Gibbs SE. Linking nucleus accumbens dopamine and blood oxygenation. Psychopharmacology (Berl). 2007; 191(3):813–822. [PubMed: 17279377]
22. Chen YC, Choi JK, Andersen SL, Rosen BR, Jenkins BG. Mapping dopamine D2/D3 receptor function using pharmacological magnetic resonance imaging. Psychopharmacology (Berl). 2004; 180(4):705–715.
23. Marota JJ, Mandeville JB, Weisskoff RM, Moskowitz MA, Rosen BR, Kosofsky BE. Cocaine activation discriminates dopaminergic projections by temporal response: an fMRI study in Rat. Neuroimage. 2000; 11(1):13–23. [PubMed: 10686113]
24. Underhill SM, Wheeler DS, Li M, Watts SD, Ingram SL, Amara SG. Amphetamine modulates excitatory neurotransmission through endocytosis of the glutamate transporter EAAT3 in dopamine neurons. Neuron. 2014; 83(2):404–416. [PubMed: 25033183]
25. Schultz W. Predictive reward signal of dopamine neurons. Journal of Neurophysiology. 1998; 80(1):1–27. [PubMed: 9658025]
26. Mandeville JB, Marota JJ. Vascular filters of functional MRI: spatial localization using BOLD and CBV contrast. Magnetic resonance in medicine : official journal of the Society of Magnetic Resonance in Medicine / Society of Magnetic Resonance in Medicine. 1999; 42(3):591–598.
27. Zhao F, Wang P, Hendrich K, Ugurbil K, Kim S-G. Cortical layer-dependent BOLD and CBV responses measured by spin-echo and gradient-echo fMRI: Insights into hemodynamic regulation. NeuroImage. 2006; 30(4):1149–1160. [PubMed: 16414284]
28. Poplawsky AJ, Fukuda M, Murphy M, Kim SG. Layer-Specific fMRI Responses to Excitatory and Inhibitory Neuronal Activities in the Olfactory Bulb. J Neurosci. 2015; 35(46):15263–15275. [PubMed: 26586815]
29. Witten IB, Steinberg EE, Lee SY, Davidson TJ, Zalocusky KA, Brodsky M, et al. Recombinase-driver rat lines: tools, techniques, and optogenetic application to dopamine-mediated reinforcement. Neuron. 2011; 72(5):721–733. [PubMed: 22153370]
30. Paxinos, G., Watson, C. The rat brain in stereotaxic coordinates. 6. Elsevier Academic Press; New York: 2007.
31. Silva AC, Koretsky AP, Duyn JH. Functional MRI impulse response for BOLD and CBV contrast in rat somatosensory cortex. Magnetic resonance in medicine : official journal of the Society of

Author Manuscript Author Manuscript Author Manuscript Author Manuscript

Magnetic Resonance in Medicine / Society of Magnetic Resonance in Medicine. 2007; 57(6): 1110–1118.

32. Kim SG, Harel N, Jin T, Kim T, Lee P, Zhao F. Cerebral blood volume MRI with intravascular superparamagnetic iron oxide nanoparticles. NMR Biomed. 2013; 26(8):949–962. [PubMed: 23208650]
33. Cox RW. AFNI: Software for Analysis and Visualization of Functional Magnetic Resonance Neuroimages. Computers and Biomedical Research. 1996; 29(3):162–173. [PubMed: 8812068]
34. Kim T, Masamoto K, Fukuda M, Vazquez A, Kim SG. Frequency-dependent neural activity, CBF, and BOLD fMRI to somatosensory stimuli in isoflurane-anesthetized rats. Neuroimage. 2010; 52(1):224–233. [PubMed: 20350603]
35. Swanson L. The projection of the ventral tegmental area and adjacent regions: a combined fluorescent retrograde tracer and immunofluorescence study in the rat. Brain Research Bulletin. 1982; 9:321–353. [PubMed: 6816390]
36. Berger B, Casper P, Verney C. Dopaminergic innervation of the cerebral cortex: Unexpected differences between rodents and primates. TINS. 1991; 14:21–27. [PubMed: 1709528]
37. Klitenick MA, Deutch AY, Churchill L, Kalivas PW. Topography and functional role of dopaminergic projections from the ventral mesencephalic tegmentum to the ventral pallidum. Neuroscience. 1992; 50(2):371–386. [PubMed: 1279461]
38. Yetnikoff L, Lavezzi HN, Reichard RA, Zahm DS. An update on the connections of the ventral mesencephalic dopaminergic complex. Neuroscience. 2014; 282C:23–48.
39. Liljeholm M, O'Doherty JP. Contributions of the striatum to learning, motivation, and performance: an associative account. Trends Cogn Sci. 2012; 16(9):467–475. [PubMed: 22890090]
40. Van Waes V, Beverley JA, Siman H, Tseng KY, Steiner H. CB1 Cannabinoid Receptor Expression in the Striatum: Association with Corticostriatal Circuits and Developmental Regulation. Front Pharmacol. 2012; 3:21. [PubMed: 22416230]
41. Boyden ES, Zhang F, Bamberg E, Nagel G, Deisseroth K. Millisecond-timescale, genetically targeted optical control of neural activity. Nat Neurosci. 2005; 8(9):1263–1268. [PubMed: 16116447]
42. Beier Kevin T, Steinberg Elizabeth E, DeLoach Katherine E, Xie S, Miyamichi K, Schwarz L, et al. Circuit Architecture of VTA Dopamine Neurons Revealed by Systematic Input-Output Mapping. Cell. 2015; 162(3):622–634. [PubMed: 26232228]
43. Bass CE, Grinevich VP, Gioia D, Day-Brown JD, Bonin KD, Stuber GD, et al. Optogenetic stimulation of VTA dopamine neurons reveals that tonic but not phasic patterns of dopamine transmission reduce ethanol self-administration. Front Behav Neurosci. 2013; 7:173. [PubMed: 24324415]
44. Tritsch NX, Ding JB, Sabatini BL. Dopaminergic neurons inhibit striatal output through non-canonical release of GABA. Nature. 2012; 490(7419):262–266. [PubMed: 23034651]
45. Tritsch NX, Oh WJ, Gu C, Sabatini BL. Midbrain dopamine neurons sustain inhibitory transmission using plasma membrane uptake of GABA, not synthesis. Elife. 2014; 3:e01936. [PubMed: 24843012]
46. Iordanova B, Vazquez AL, Poplawsky AJ, Fukuda M, Kim S-G. Neural and hemodynamic responses to optogenetic and sensory stimulation in the rat somatosensory cortex. J Cereb Blood Flow Metab. 2015; 35(6):922–932. [PubMed: 25669905]
47. Sibson NR, Dhankhar A, Mason GF, Rothman DL, Behar KL, Shulman RG. Stoichiometric coupling of brain glucose metabolism and glutamatergic neuronal activity. Proc Natl Acad Sci U S A. 1998; 95(1):316–321. [PubMed: 9419373]
48. Haber SN, Calzavara R. The cortico-basal ganglia integrative network: the role of the thalamus. Brain research bulletin. 2009; 78(0):69–74. [PubMed: 18950692]
49. Voorn P, Vanderschuren LJ, Groenewegen HJ, Robbins TW, Pennartz CM. Putting a spin on the dorsal-ventral divide of the striatum. Trends Neurosci. 2004; 27(8):468–474. [PubMed: 15271494]
50. Nauta WJH, Smith GP, Faull RLM, Domesick VB. Efferent connections and nigral afferents of the nucleus accumbens septi in the rat. Neuroscience. 1978; 3(4–5):385–401. [PubMed: 683502]

Author Manuscript Author Manuscript Author Manuscript Author Manuscript

51. Helbing C, Brocka M, Scherf T, Lippert MT, Angenstein F. The role of the mesolimbic dopamine system in the formation of blood-oxygen-level dependent responses in the medial prefrontal/anterior cingulate cortex during high-frequency stimulation of the rat perforant pathway. Journal of Cerebral Blood Flow & Metabolism. 2015
52. Matsumoto M, Hikosaka O. How do dopamine neurons represent positive and negative motivational events? Nature. 2009; 459(7248):837–841. [PubMed: 19448610]
53. Csernansky JG, Bardgett ME. Limbic-cortical neuronal damage and the pathophysiology of schizophrenia. Schizophr Bull. 1998; 24(2):231–248. [PubMed: 9613623]
54. Kumari V, Gray JA, Honey GD, Soni W, Bullmore ET, Williams SCR, et al. Procedural learning in schizophrenia: a functional magnetic resonance imaging investigation. Schizophrenia Research. 2002; 57(1):97–107. [PubMed: 12165380]
55. Reiss JP, Campbell DW, Leslie WD, Paulus MP, Ryner LN, Polimeni JO, et al. Deficit in schizophrenia to recruit the striatum in implicit learning: A functional magnetic resonance imaging investigation. Schizophrenia Research. 2006; 87(1–3):127–137. [PubMed: 16814986]
56. Murray GK, Corlett PR, Clark L, Pessiglione M, Blackwell AD, Honey G, et al. Substantia nigra/ventral tegmental reward prediction error disruption in psychosis. Molecular psychiatry. 2008; 13(3):239–276. [PubMed: 17684497]
57. Weickert TW, Goldberg TE, Callicott JH, Chen Q, Apud JA, Das S, et al. Neural correlates of probabilistic category learning in patients with schizophrenia. The Journal of neuroscience : the official journal of the Society for Neuroscience. 2009; 29(4):1244–1254. [PubMed: 19176832]
58. Kegeles LS, Abi-Dargham A, Frankle WG, Gil R, Cooper TB, Slifstein M, et al. Increased synaptic dopamine function in associative regions of the striatum in schizophrenia. Arch Gen Psychiatry. 2010; 67(3):231–239. [PubMed: 20194823]
59. Howes OD, Montgomery AJ, Asselin MC, Murray RM, Valli I, Tabraham P, et al. Elevated striatal dopamine function linked to prodromal signs of schizophrenia. Arch Gen Psychiatry. 2009; 66(1):13–20. [PubMed: 19124684]
60. Claus ED, Ewing SWF, Filbey FM, Sabbineni A, Hutchison KE. Identifying Neurobiological Phenotypes Associated with Alcohol Use Disorder Severity. Neuropsychopharmacology. 2011; 36(10):2086–2096. [PubMed: 21677649]
61. Vollstädt-Klein S, Wichert S, Rabinstein J, Bühler M, Klein O, Ende G, et al. Initial, habitual and compulsive alcohol use is characterized by a shift of cue processing from ventral to dorsal striatum. Addiction. 2010; 105(10):1741–1749. [PubMed: 20670348]
62. Lammel S, Steinberg EE, Foldy C, Wall NR, Beier K, Luo L, et al. Diversity of transgenic mouse models for selective targeting of midbrain dopamine neurons. Neuron. 2015; 85(2):429–438. [PubMed: 25611513]
63. Totah NK, Kim Y, Moghaddam B. Distinct prestimulus and poststimulus activation of VTA neurons correlates with stimulus detection. J Neurophysiol. 2013; 110(1):75–85. [PubMed: 23554430]
64. Kim YB, Matthews M, Moghaddam B. Putative gamma-aminobutyric acid neurons in the ventral tegmental area have a similar pattern of plasticity as dopamine neurons during appetitive and aversive learning. Eur J Neurosci. 2010; 32(9):1564–1572. [PubMed: 21040517]
65. Desai M, Kahn I, Knoblich U, Bernstein J, Atallah H, Yang A, et al. Mapping brain networks in awake mice using combined optical neural control and fMRI. J Neurophysiol. 2011; 105(3):1393–1405. [PubMed: 21160013]

Author Manuscript Author Manuscript Author Manuscript Author Manuscript

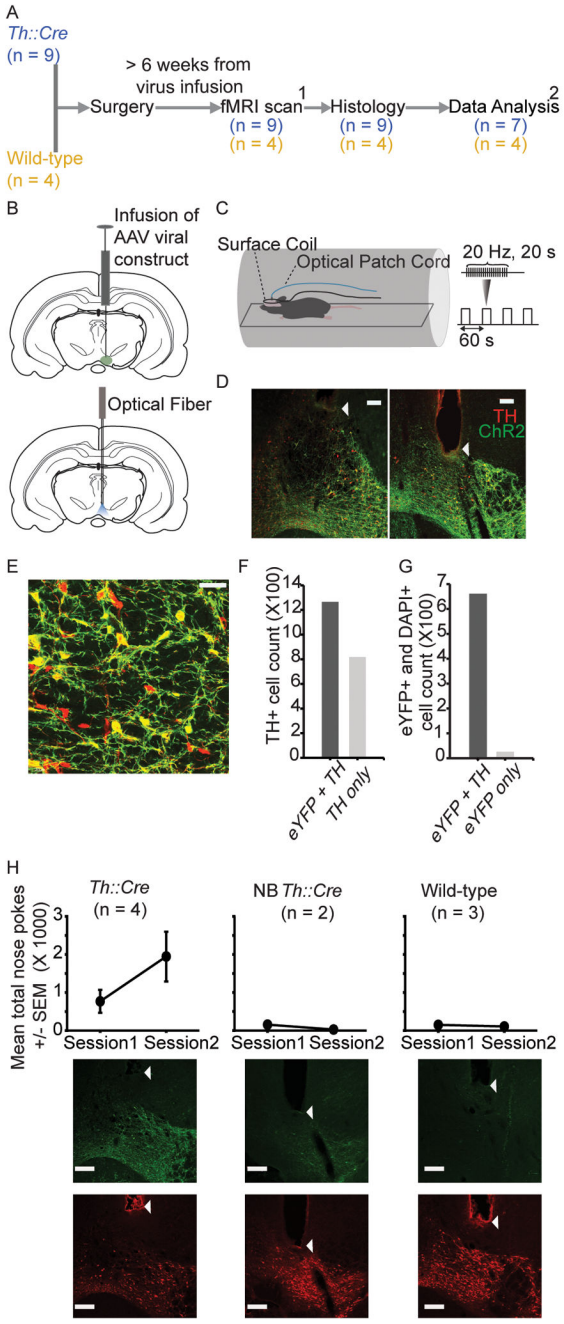

Figure 1.

Experimental design, histology and behavior. **(A)** Experimental design. [1] A subset of rats (6 *Th::Cre* and 3 wild-type) were characterized behaviorally in an intra-cranial self-stimulation (ICSS) task prior to fMRI scanning. [2] Two *Th::Cre* rats were excluded from the *Th::Cre* group fMRI data analysis due to low levels of ChR2 integration in VTA and weak expression of ICSS behavior (also see Figure 1H). **(B)** Schematic demonstrating infusion of AAV viral construct and implantation of an optical fiber in right VTA. **(C)** fMRI setup. Each fMRI run consisted of 5 s of baseline followed by 4 optical stimulation trials. In each trial,

Author Manuscript Author Manuscript Author Manuscript Author Manuscript

blue laser pulses were delivered to VTA at 20 Hz (5 ms width, power = 2.5 – 7.5 mW, 473 nm) for 20 s, followed by 40 s of rest. **(D)** Representative histological images from two *Th::Cre* rats showing ChR2 expression and implanted fiber tips (white arrowheads) in VTA. Scale bar: 130 μm. **(E)** Expression of ChR2-eYFP (green) in TH+ (red) neurons in VTA of *Th::Cre* rats. Scale bar: 40 μm. **(F)** Quantification of TH+ cell bodies (n = 2083 cells from 7 *Th::Cre* rats) that also express eYFP in VTA (measure of sensitivity of ChR2-eYFP expression). **(G)** Quantification of VTA cell bodies immunopositive for both eYFP and DAPI (n = 687 cells from 4 *Th::Cre* rats) that also express TH in VTA (measure of specificity of ChR2-eYFP expression). **(H)** (Top) ICSS behavior. Rats executed nose pokes to receive optical VTA stimulation (20 Hz, 5 ms pulse width, power = 5 – 8 mW, 473 nm). The average total number of nose pokes executed per session by *Th::Cre*, "behaviorally non-responsive" *Th::Cre* (NB *Th::Cre*) and wild-type rats is shown. (Bottom) Representative histological images show a differential amount of ChR2 (green fluorescence, top row) expression directly below the optical fiber tips in VTA of *Th::Cre,* NB *Th::Cre,* and wild-type rats. The bottom row shows TH expression in images acquired in the same field of view as the ChR2 images (top row). All images corresponding to a particular fluorescence stain (ChR2 or TH) were acquired using the same parameters, and white arrowheads point to optical fiber tips. Scale bars: 200 μm.

Author Manuscript Author Manuscript Author Manuscript Author Manuscript

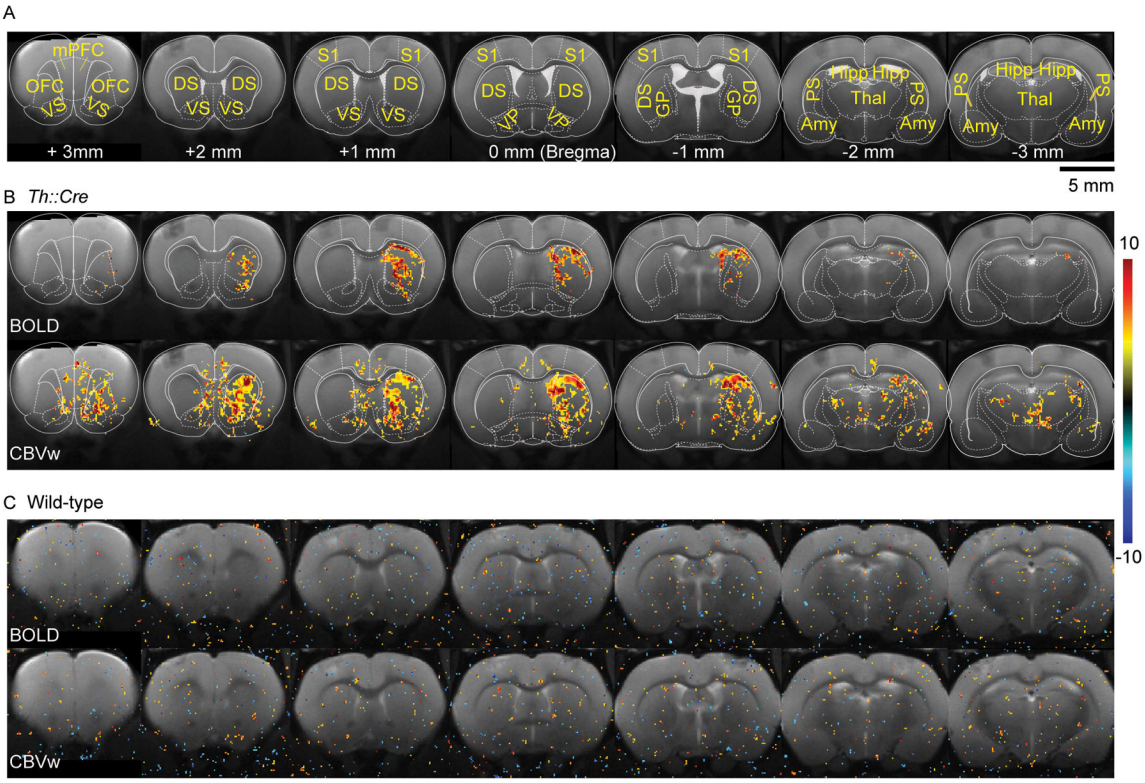

Figure 2.

Group activation maps. **(A)** Atlas figures overlaid on structural images to delineate regions-of-interest (ROIs) (mPFC = medial prefrontal cortex; OFC = orbitofrontal cortex; DS = dorsal striatum; VS = ventral striatum; S1 = primary somatosensory cortex; VP = ventral pallidum; GP = globus pallidus; Hipp = hippocampus; Amy = amygdala; Thal = thalamus; PS = posterior striatum). **(B)** Statistical t-value maps overlaid on structural images illustrate increased BOLD and CBVw activity in the striatum and other ROIs after optical VTA stimulation in *Th::Cre* rats (n = 5 for BOLD and n = 6 for CBVw). Note that positive CBVw t-values represent blood volume increases during stimulation. Atlas overlays (same as A) mark the boundaries of ROIs. Voxel-wise and family-wise error correction (cluster size > 28 voxels) thresholds were set to $p < 0.025$. (See Supplementary Figure 2 for group maps with different thresholds) **(C)** Wild-type (n = 4 for BOLD and CBVw) rats do not exhibit any increase in BOLD and CBVw activity in the whole brain even at a low threshold (voxel-level $p < 0.025$ and cluster size > 0 voxels) upon optical VTA stimulation. Color bar indicates t-values. Voxel size: 125 μm × 125 μm × 1 mm.

Author Manuscript Author Manuscript Author Manuscript Author Manuscript

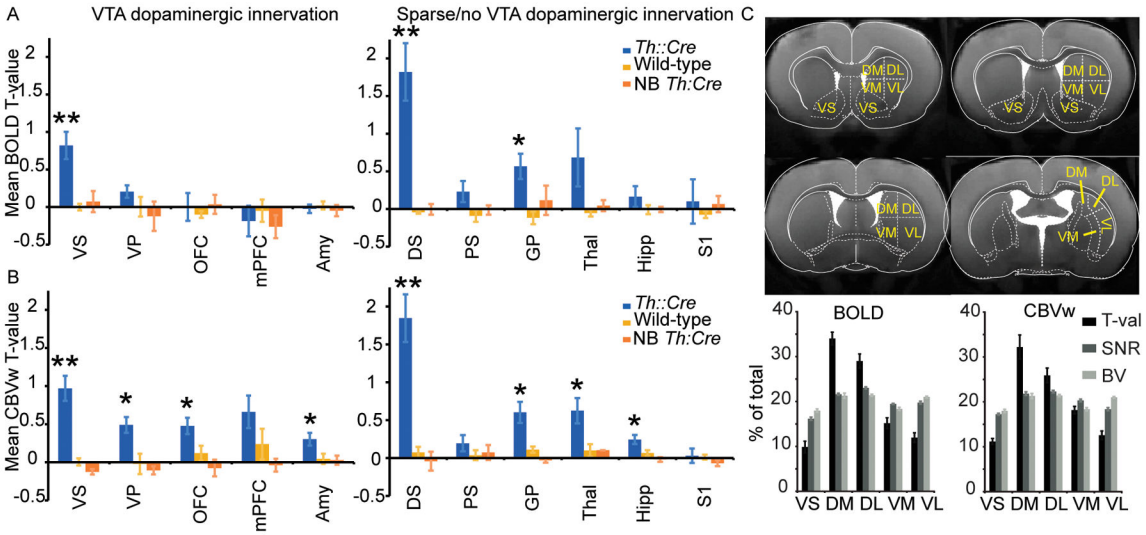

Figure 3.

Ipsilateral ROI analysis (see Supplementary Figure 4 for contralateral ROI analysis). Mean ± SEM t-values for correlation of **(A)** BOLD and **(B)** CBVw signal changes within ROIs with predicted hemodynamic response functions. Right hemisphere ROIs were drawn on individual structural images for *Th::Cre* rats (n = 5 for BOLD and n = 7 for CBVw), NB *Th::Cre* rats (n = 2 for BOLD and CBVw), and wild-type rats (n = 4 for BOLD and CBVw). Brown-Forsythe ANOVAs yielded significant differences in activation t-values for BOLD in the following ROIs: **VS** ($F(2,8) = 13.569$, $p = 0.008$), **DS** ($F(2,8) = 23.017$, $p = 0.006$), and **GP** ($F(2,8) = 6.843$, $p = 0.043$) and for CBVw in the following structures: **VS** ($F(2,10) = 34.546$, $p = 0.000$), **VP** ($F(2, 10) = 10.625$, $p = 0.006$), **OFC** ($F(2,10) = 7.4555$, $p = 0.015$), **amygdala** ($F(2,10) = 5.489$, $p = 0.025$), **DS** ($F(2, 10) = 29.262$, $p = 0.000$), **GP** ($F(2,10) = 14.061$, $p = 0.003$), **thalamus** ($F(2,10) = 8.131$, $p = 0.012$), and **hippocampus** ($F(2,10) = 8.624$, $p = 0.007$). Post-hoc two sample t-tests resulted in significant differences in BOLD t-values between *Th::Cre* and wild-type rats in these ROIs: **VS** ($t(7) = 4.376$, $p = 0.009$), **DS** ($t(7) = 4.879$, $p = 0.008$), and **GP** ($t(7) = 3.643$, $p = 0.012$). CBVw t-values were significantly different between *Th::Cre* and wild-type rats in these ROIs: **VS** ($t(9) = 5.639$, $p = 0.001$), **VP** ($t(9) = 3.013$, $p = 0.021$), **OFC** ($t(9) = 2.460$, $p = 0.038$), **amygdala** ($t(9) = 2.409$, $p = 0.040$), **DS** ($t(9) = 5.472$, $p = 0.001$), **GP** ($t(9) = 3.397$; $p = 0.012$)**, thalamus** ($t(9) = 2.817$, $p = 0.022$), and **hippocampus** ($t(9) = 2.523$, $p = 0.033$). There was no significant difference between NB *Th::Cre* and wild-type groups for any ROI. * = $p < 0.05$, ** = $p < 0.01$. **(C)** DS of *Th::Cre* rats was divided into four quadrants (DM = dorsomedial, DL = dorsolateral, VM = ventromedial, and VL = ventrolateral) as indicated in the anatomical images with overlaid atlas figures (top). BOLD and CBVw t-values, BOLD and CBVw baseline signal-to-noise ratio (SNR), and baseline blood volume (BV) were expressed as percentages of summed total values across the five subdivisions of striatum, including VS (bottom). One-way repeated measures ANOVAs yielded significant differences among sub-divisions of the striatum in relative activation t-values for BOLD ($F(4, 16) = 53.067$, $p = 0.000$, n = 5 rats) and CBVw ($F(4, 24) = 26.913$, $p = 0.000$, n = 7 rats, Greenhouse-Geisser corrected) contrasts. Repeated measures ANOVAs also resulted in significant differences

Author Manuscript Author Manuscript Author Manuscript Author Manuscript

among striatal subdivisions in relative BV ($F(4, 24) = 16.623$, $p = 0.000$, $n = 7$ rats) and relative SNR for BOLD ($F(4, 16) = 76.71$, $p = 0.000$, $n = 5$ rats) and CBVw ($F(4, 24) = 37.34$, $p = 0.000$, $n = 7$ rats) contrasts.

Author Manuscript Author Manuscript Author Manuscript Author Manuscript

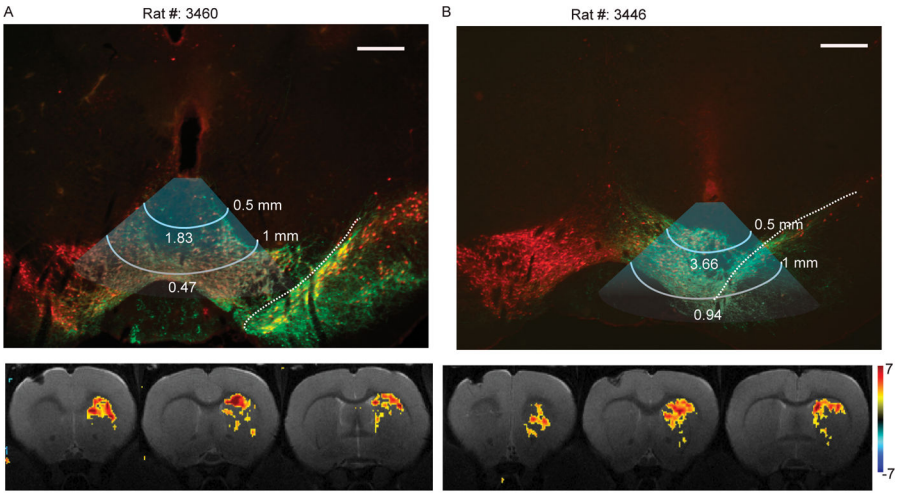

Figure 4.

Individual histology and activation maps. (Top) Schematics of approximate spread of blue light in the VTA and SN are overlaid on immunohistological images (red: TH, green: ChR2-eYFP) that show optical fiber tips at locations farthest from SN **(A)** and closest to SN **(B)**. The predicted irradiance values (mW/mm^2) calculated using the online irradiance calculator (http://www.stanford.edu/group/dlab/cgi-bin/graph/chart.php) are indicated for distances of 0.5 mm (first white line) and 1 mm (second white line) from the optical fiber tips. Scale bar: 0.5 mm. Dashed white lines mark the approximate boundary between VTA and SN. (Bottom) CBVw t-value statistical maps for two rats (A and B) illustrate individual responses in the striatum to VTA optical stimulation. Voxel-wise and family-wise error correction (cluster size > 19 voxels) thresholds were set to $p < 0.01$. Color bar: t-values.